Summer Project

Astral Trails

Midterm Report

Mentors:

Chhavi Tanwar
Tanmay Rajput
Akshat Dhote
Aditya Prakhar

Mentees:

Antriksh Singhal
Rucha Pimpalkar
Aditi Yadav
Harpuneet Singh
Akshita Vinit Dixit
Iqra Afreen
Sunand Garg
Kanishk Sharma
Ayush Kumar Singh
Aditya Krishna
Mahi Mittal
Mishthi Sharma
Srushti Jagtap
Daksh Nandan Singh
Manan Gagrani
Vansh Sejpal
Priyam
Shlok Sharma
Nikhil Kumar

Contents

Abstract

The Astral Trails Project aims to develop a cloud chamber to trace the paths of cosmic rays passing through it. By making invisible high-energy particles visible, the project serves as a stepping stone toward understanding space radiation and its implications for future space exploration. This document outlines the goals, methodology, and results of our research and design process.

Chapter 1

Introduction

1.1 Motivation

The motivation for the Astral Trails project stems from the need to analyze the interactions and potential biological effects of cosmic rays. This is especially relevant given the growing accessibility of space travel and the advent of long-term human missions beyond Earth's protective atmosphere. Unlike Earth, spacecraft and planetary bases offer limited shielding against high-energy cosmic radiation, making it a significant concern for astronaut health and mission safety.

Understanding cosmic rays is essential not only for mitigating radiation risks in space but also for advancing our knowledge of high-energy astrophysical phenomena. Moreover, studying cosmic radiation can inform the development of better shielding materials, early-warning systems for solar particle events, and models of radiation exposure. By constructing a cloud chamber to visualize these particles, we aim to contribute to the broader effort of preparing for the challenges posed by space environments.

1.2 Objectives

The primary objectives of the Astral Trails Project are as follows:

- **Understanding Cosmic Rays:** Learn about the origin of cosmic rays, their constituent particles, and their effects on DNA and Computers.
- **Cloud Chamber Design:** Develop a simple yet accurate model of a Diffusion Cloud Chamber to make visible trails.
- **Computer Vision:** Analyse the tracks using Computer Vision (OpenCV) to automatically classify cosmic rays based on their constituent particles.
- **DNA Mutation:** Model the effects of Cosmic Rays on DNA to learn more about the impact of long-term space missions on the human body.

1.3 Scope

The scope of this project includes the following key areas:

- **Structural Design:** Develop a stable and compact cloud chamber that is structurally sound, cost-effective, and suitable for sustained observation.
- **Particle Detection:** Enable real-time visualization of ionizing particles by optimizing conditions for track formation, such as temperature gradients and alcohol vapor saturation.
- **Material Selection:** Identify and integrate appropriate materials (e.g., acrylic sheets and felt) to ensure durability, visibility, and effective condensation.

- **Thermal System Engineering:** Design a cooling system (using silicon gel cooling pads) capable of maintaining the sub-zero temperatures required for supersaturation inside the chamber.
- **Biological Impact Assesment:** Explore the implications of cosmic ray exposure on biological systems by studying existing research on DNA damage, mutations, and carcinogenesis caused by ionizing radiation.

1.4 Significance

The significance of the Astral Trails project lies in its contribution to understanding the fundamental nature of cosmic radiation and its potential effects on human health, especially in the context of long-duration space missions. By enabling the direct observation of cosmic ray interactions through a cloud chamber, the project provides an accessible platform for studying high-energy particles that are otherwise invisible. This research not only supports the future of safe space travel but also fosters public interest in particle physics and astrophysics. Additionally, insights gained from radiation exposure studies may have broader applications in medical imaging, radiation therapy, and radiation shielding technologies on Earth.

Chapter 2

Background and Literature Review

2.1 History of Cosmic Rays

Cosmic rays are messengers from the vast extents of space, carrying valuable information about their sources and the space they travel though. The term was coined by physicist Robert Millikan in 1925. Victor Hess discovered cosmic rays for the first time in 1912 during his balloon experiments.

B. Rossi and A. Piccard (1930s) worked on cosmic rays, paving the way for later discoveries of sub-atomic particles within cosmic ray showers. Walter Baade and Fritz Zwicky (1934) as well as Enrico Fermi (1949), hypothesized the origin of these rays, suggesting origin from supernovae and other extra-galactic sources. The origin of UHECRs remains an active area of research in Astrophysics.

2.2 History of the Cloud Chamber

The cloud chamber are an indispensable tool in the field of nuclear and particle physics, allowing scientists to observe phenomena that were previously completely theoretical directly. Particles such as electrons, positrons, alpha particles, and so on produce visible paths inside a cloud chamber.

Wilson's (1911) original design of an expansion chamber was intended to visualize cloud formation, which led to the accidental discovery. Wilson went on to improve and perfect the design of his cloud chamber. American physicist Carl Anderson (1932-1936) discovered the positron (1932) and muon (1936) using cloud chambers.

2.3 Referenced Literature

The various types of cloud chambers are as follows:

- Measurement of Cloud Properties Using a Self-Designed Cloud Chamber - Ridhesh Goti1, Bhashin Thakore1, and Rohit Srivastava
- The Cloud Chamber Experiment - Ken Clark January 3, 2019
- Tronic Cloud Chamber - refrigeration based miniaturized cloud chamber - Sanjay Lakshminarayana

Chapter 3

Astronomy 101

3.1 History

- **Pythagoras**
  - He believed that everything was related to mathematics and that through mathematics, everything could be predicted and measured in rhythmic patterns or cycles.
  - Pythagoras placed astronomy as one of the four mathematical arts, the others being arithmetic, geometry and music.

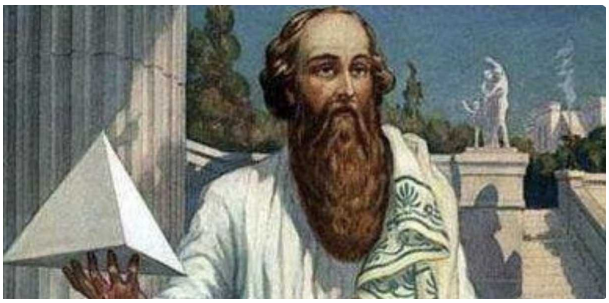

Figure 3.1: Pythagoras

- **Aristotle**
  - The Earth was in the center, and the Sun, the Moon, the stars, and the planets orbited on separate spheres that encased each other and spun at different rates (Geocentric Model).

- Motion caused by a supernatural being.
- Earth was a sphere (could see shadow on moon during eclipse) and non-moving (because we could not feel it and falling objects would not drop straight down).

Figure 3.2: Pythagoras

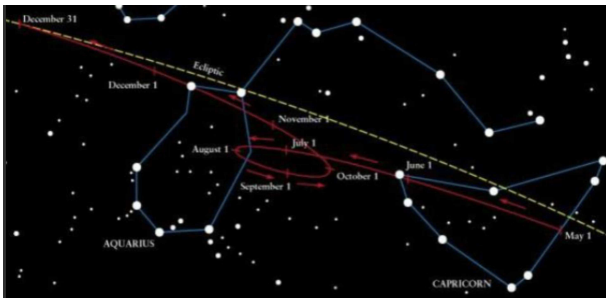

- **Ptolemy**
  - Geo-centric model
  - Each planet was fixed to a small sphere that was fixed to a larger sphere (epicycles).
  - No changes made for a 1,000 years until the inaccuracies in predictions became too big to blame on primitive equipment

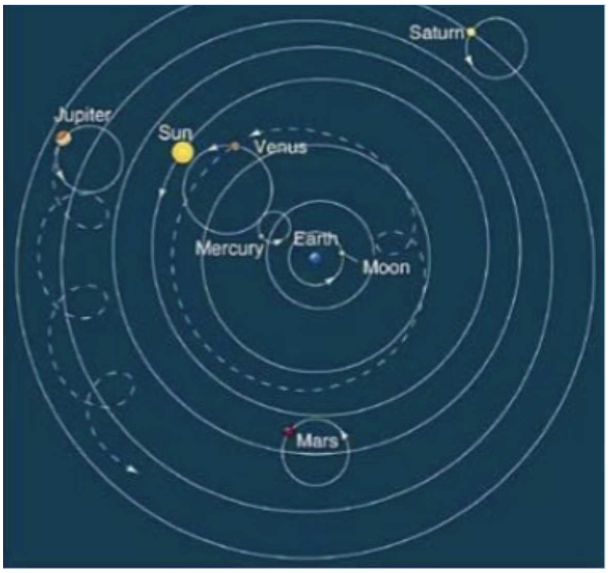

Figure 3.3: Geocentric model

- **Copernicus**
  - Introduced a sun centered design of the Universe called the Heliocentric View.
  - Therefore, Ptolemy's astronomy was seriously questioned and eventually overthrown
- **Tycho Brahe**
  Tycho Brahe's major contributions were:-
  - The detection and correction of several serious errors in the standard astronomical tables.
  - The discovery of a supernova in the constellation of Cassiopeia.
  - The most complete and accurate observations available without the use of a telescope.
- **Kepler**
  Tycho's assistant, Kepler had full access to Tycho's data. He determined that the orbits were not circular but elliptical.

  Kepler's Three Laws of Planetary Motion:

- The orbits of the planets are elliptical.
- The earth's orbital speed varies at different times of the year. The earth moves fastest in its orbit when closest to the sun and slowest when farthest away.
- Shows the relationship between the size of a planet's orbit radius and its orbital period

- **Galileo**
  - He provided the crucial observations that proved the Copernican hypothesis.
  - Galileo used his telescope to show errors in Aristotle's opinion of the universe and the worldview that it supported.

- **Sir Isaac Newton**
  - Built on Galieo's ideas to demonstrate that the laws of motion in the heavens and on Earth were the same.
  - Newton completed the synthesis of astronomy and physics.
  - He gave reasons for and corrected Kepler's Laws and came up with three new Laws of Motion based on his idea of the existence of a force called 'Gravity'

- **Edwin Hubble**
  - Was able to measure the distance to observed celestial objects.
  - He discovered that the Milky Way was only one of many galaxies.
  - Provided evidence to suggest that most distance galaxies were moving away from us.

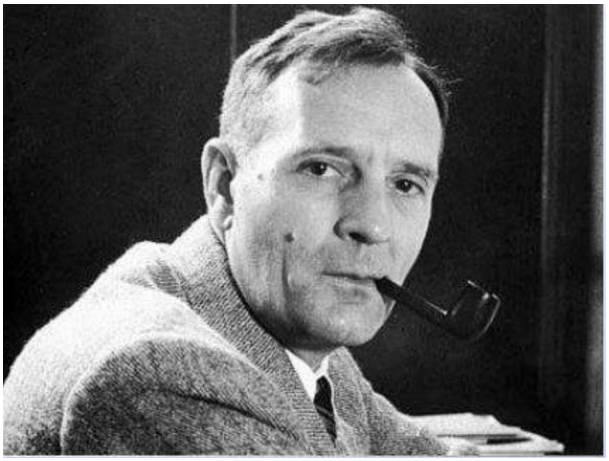

Figure 3.4: Edwin Hubble

- **Georges Lemaitre**
  - A Belgian priest, astronomer and professor of physics.
  - Suggested that the Universe must be expanding.
  - His theory, supported by Hubble's work, suggested that the Universe must have begun as a small, extremely dense point of matter.
  - Lemaitre's theory is famously called the "Big Bang Theory"

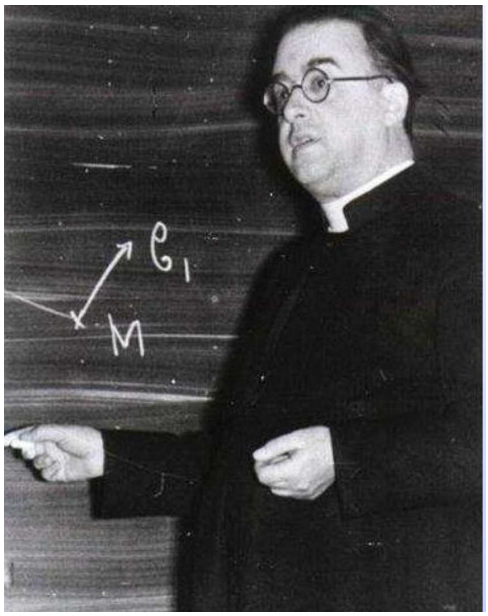

Figure 3.5: Georges Lemaitres

3.2 Domains

- **Theoretical Astronomy**
  Theoretical astronomy is a branch of astronomy that uses physics and chemistry to create models that explain astronomical phenomena. Theoretical astronomers use analytical models and computational simulations to describe astronomical objects and phenomena.
- **Computational Astronomy**
  - Huge amounts of data to process
  - Time Series Analysis
  - Simulations for easy understanding
  - Models for analysis
  - Image enhancement and pre processing
- **Radio Astronomy**
  Radio astronomy is the study of celestial objects and phenomena by using radio waves. It involves collecting and analyzing data from radio telescopes to gain insights into the universe. Radio astronomers convert the numbers collected by a telescope into pictures. Each number represents information from a specific point in space.
- **Observational Astronomy**
  Observational astronomy is focused on acquiring data from observations of astronomical objects. This data is then analyzed using basic principles of physics.

3.3 Coordinate System

Coordinate systems are used for specifying positions of celestial objects (satellites, planets, stars, galaxies, etc.) relative to a given reference frame.

3.3.1 Types of coordinate systems

- Equatorial coordinate system

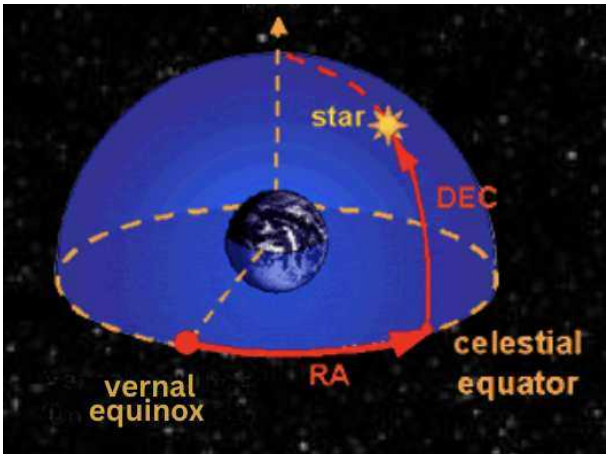

Figure 3.6: Equatorial coordinate system

- Altitude-Azimuth coordinate system

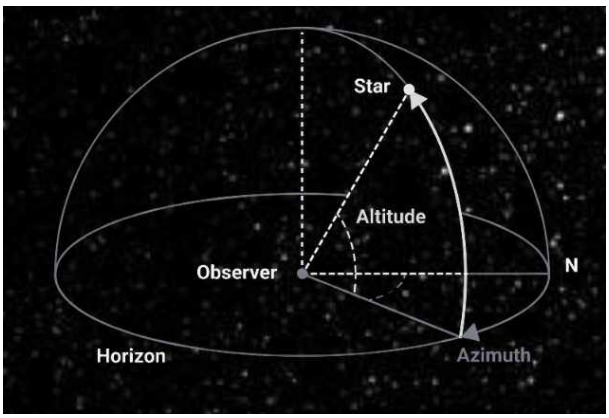

Figure 3.7: Altitude-Azimuth coordinate system

- Ecliptic Coordinate system

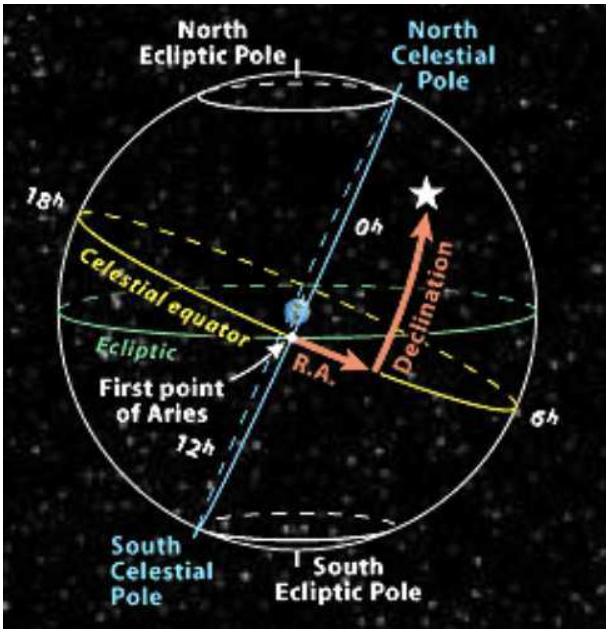

Figure 3.8: Ecliptic Coordinate system

- Galactic coordinate system
- Supergalactic Coordinate system

3.4 Stellar Life Cycle

3.4.1 Introduction

Stars are massive celestial bodies composed primarily of hydrogen and helium, undergoing nuclear fusion that emits light and heat. The evolution of a star depends largely on its initial mass, determining whether it ends its life as a white dwarf, neutron star, or black hole.

3.4.2 Star Formation

Stars form in stellar nebulae, which are vast clouds of gas and dust. Under the influence of gravity, regions within the nebula collapse and condense, increasing in temperature and pressure. As it continues to contract, its rotational forces it into a disk shape. This is called a protostar.

As it continues to contract and heat up, fusion of hydrogen into helium begins in its core. Once fusion stabilizes, the star enters the main sequence phase.

3.4.3 Red Giant or Supergiant (Depending on Mass)

- Low to Medium mass stars: Expand into red giants as hydrogen is depleted and helium fusion begins.
- High mass stars: Become supergiants and undergo fusion of heavier elements up to iron.

3.4.4 Final stages

Low to medium mass stars:

- Planetary Nebula: The outer layers are ejected, leaving a glowing shell of ionized gas. These play a part in planet formation, thus the name.
- White Dwarf: These stars no longer undergo fusion and are extremely dense, composed mainly of carbon and oxygen.
- Black Dwarf: It is theorised that white dwarves cool down, over a very long time period, to end up as black dwarves. This time is theorised to be so long that the universe is not old enough to have formed these stars.

High mass stars:

- Supernova: A massive explosion triggered when the iron core collapses as gravity dominates. Elements beyond Iron are produced during this explosion.
- Neutron Star: On the lower side of the Chandrasekhar Limit (with a core under 3 Solar masses), Neutron stars are born.

They are so extremely dense that protons and electrons merge into neutrons. It is hypothesized that exotic matter is found in their cores.

- Black Holes: Stars having core masses beyond 3 Solar masses are overtaken by gravity and collapse into a singularity. Their gravity is so extreme that not even light can escape their gravity, once it crosses the event horizon. Due to this nature, most of their physics lies unknown.

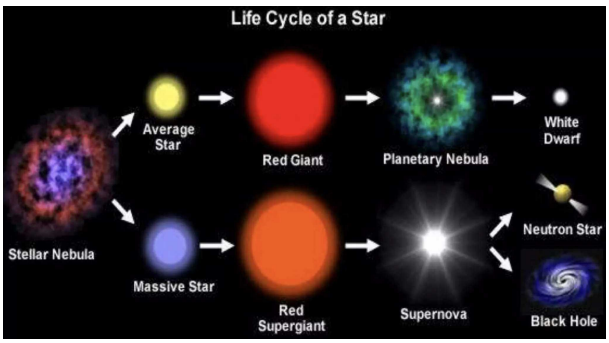

Figure 3.9: Stellar Cycle

3.4.5 Other Celestial objects

- Pulsars: Pulsars are rapidly rotating neutron stars that emit beams of electromagnetic radiation. The apparent pulsing is when these beams sweep across Earth and are detectable by our sensors.

- Magnetars: Magnetars are a type of neutron star characterized by extremely powerful magnetic fields, far exceeding those of typical neutron stars. These intense magnetic fields drive the emission of high-energy electromagnetic radiation, particularly X-rays and gamma rays. They are believed to be the source of some of the most energetic bursts observed in the universe, such as soft gamma repeaters and anomalous X-ray pulsars.

Chapter 4

Introduction to Cosmic Rays

4.1 What are cosmic rays?

Cosmic rays are high-energy particles originating from outer space that travel through the universe at relativistic speeds. These particles come from outer space (the 'cosmos') and our solar system. Scientists first called these particles "rays" because they thought they were a form of electromagnetic radiation. But they are not rays at all - they're particles! They consist predominantly of protons and atomic nuclei.

4.1.1 Primary Cosmic Rays

The primary cosmic rays, which travel through space before hitting Earth's atmosphere, are composed mostly of protons ($\sim$90%), followed by alpha particles or helium nuclei ($\sim$9%), and a small fraction ($\sim$1%) of heavier nuclei like carbon, oxygen, and iron. Electrons make up about 1%, while antiparticles such as positrons and antiprotons are present only in trace amounts. Lower-energy CRs are common, while high-energy CRs are rare.

4.1.2 Secondary Cosmic Rays:

When these primary particles collide with atoms in Earth's atmosphere, they produce secondary cosmic rays. They contain "shower particles". These include pions, muons, electrons, positrons, neutrinos, gamma rays, and neutrons. Can travel faster than the speed of light in air (still slower than the speed of light in a vacuum). Among these, muons are particularly notable (about 150 muons strike every square meter of the Earth every second) because they are highly penetrating and often reach the Earth's surface, where they can be detected.

4.1.3 UHECRs (Ultra High Energy Cosmic Rays)

Ultra-High Energy Cosmic Rays are defined as cosmic ray particles with energies greater than 10^{18} eV, representing the highest energy particles ever detected in nature. To put this energy scale in perspective, a single UHECR particle carries energy equivalent to a baseball travelling at approximately 100 kilometres per hour, concentrated into a subatomic particle. The most energetic UHECRs detected have reached energies approaching 10^{20} eV, pushing the boundaries of known physical processes.

Unlike lower-energy cosmic rays that are significantly deflected by galactic and intergalactic magnetic fields, UHECRs travel in relatively straight trajectories due to their enormous energies. This unique characteristic makes them invaluable astronomical messengers, as their arrival directions can potentially point back toward their cosmic sources with minimal deflection.

Potential Sources

- Colliding Galaxies
- Magnetars (super magnetized spinning neutron stars)
- GBRs
- Giant Black holes spinning rapidly

Problems

- UHECRs are extremely rare, with flux rates at energies above 10^{19} eV dropping to approximately one particle per square kilometre per century. This rarity necessitates detector arrays covering thousands of square kilometres and long observation periods for statistically significant data.
- The Greisen-Zatsepin-Kuzmin (GZK) effect predicts that UHECRs above 6×10^{19} eV should interact with cosmic microwave background photons, causing rapid energy loss over distances greater than approx. 50 megaparsecs.
  This should create a sharp spectral cutoff, but observational evidence remains ambiguous, with some measurements showing continued flux above the predicted threshold. This GZK paradox challenges our understanding of UHECR propagation and sources.
- No known astrophysical object or process has been conclusively demonstrated to accelerate particles to energies exceeding 10^{20} eV.

4.2 What can we learn from them?

Answer: What are the elements in the universe?

Cosmic Ray Spallation Process

- When cosmic rays (primarily protons and alpha particles) collide with other atoms in space, they fragment into lighter elements.
- This process creates lithium, beryllium, and boron – elements that are rare in normal stellar processes.

Observational Evidence

- There are more cosmic rays of certain elements (Li, Be, B) than there should be based on stellar nucleosynthesis alone.
- These "excess" light elements are produced by cosmic ray collisions during space travel.

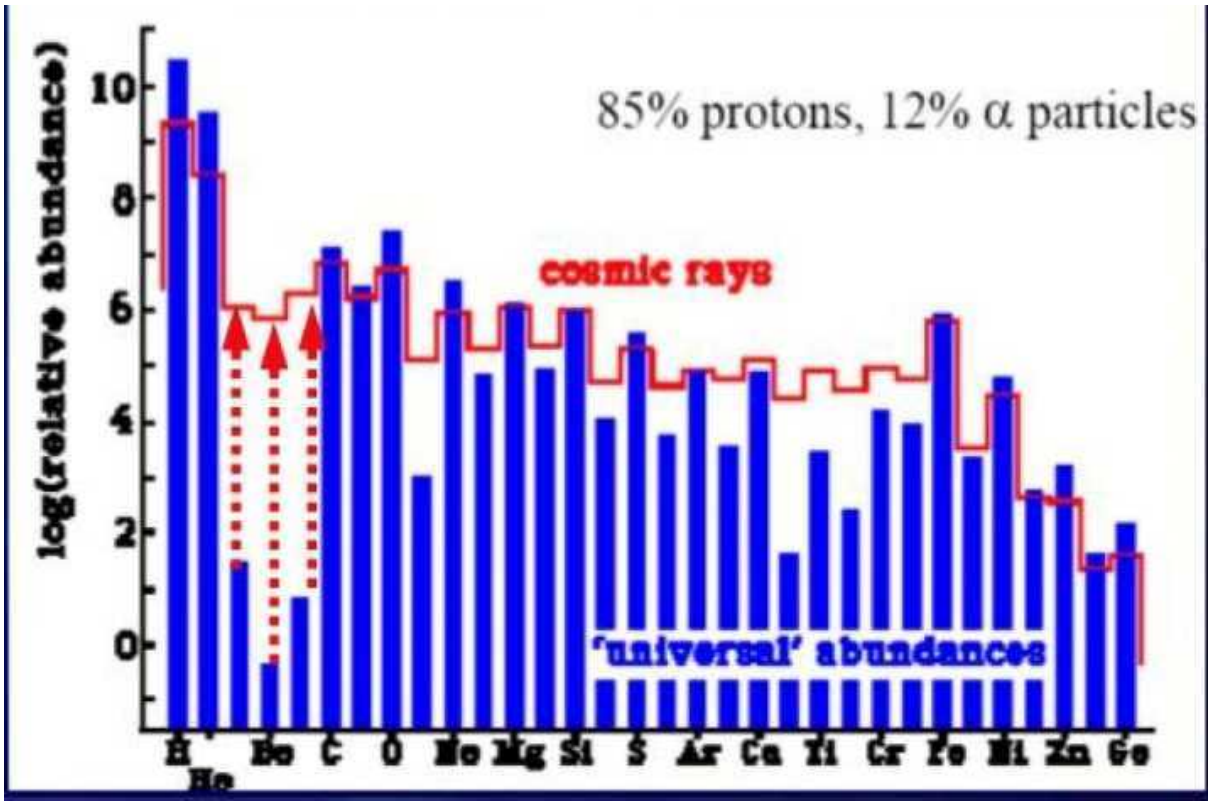

Figure 4.1: Abundance of cosmic ray elements compared to universal abundances. Excess of light elements (Li, Be, B) due to spallation is evident.

4.3 Where do they come from?

Cosmic rays originate from a variety of astrophysical sources across a wide energy spectrum. These sources can be classified by the energy level of the cosmic rays they produce:

Low-Energy Cosmic Rays

- Produced by stars.
- Example: The solar wind emitted by our Sun, which ejects protons, alpha particles, and other subatomic particles.
- These represent the lower end of the cosmic ray energy spectrum.

Medium-Energy Cosmic Rays

- Produced by supernovae — massive stellar explosions.
- These events create shock waves that accelerate particles to moderate energies through shock acceleration mechanisms.

Ultra-High Energy Cosmic Rays (UHECRs)

UHECRs are defined as cosmic ray particles with energies greater than 10^{18} eV. These are the most energetic particles ever detected in nature. To contextualize this energy:
A single UHECR particle can carry as much energy as a baseball traveling at approximately 100 km/h — but concentrated into a single subatomic particle.
The most energetic UHECRs observed have reached up to 10^{20} eV, far exceeding the energies producible by human-made particle accelerators.

Unique Characteristics:

- Due to their enormous energies, UHECRs are less deflected by galactic and intergalactic magnetic fields.
- Their relatively straight-line trajectories make them valuable as astronomical messengers, potentially pointing directly back to their sources.

Potential Sources of UHECRs:

- Colliding galaxies
- Magnetars (super-magnetized spinning neutron stars)
- Gamma-ray bursts (GRBs)
- Rapidly spinning supermassive black holes

Challenges in UHECR Detection:

- UHECRs are extremely rare: above 10^{19} eV, the flux rate drops to approximately one particle per square kilometre per century.
- Detecting them requires massive detector arrays spanning thousands of square kilometres, along with long-term observation campaigns.

The GZK Cutoff and the Paradox

Greisen–Zatsepin–Kuzmin (GZK) Effect:

- Predicts that UHECRs with energies above 6×10^{19} eV should lose energy rapidly through interactions with cosmic microwave background (CMB) photons.
- These interactions limit their effective propagation distance to around 50 megaparsecs.

GZK Paradox:

- Observations have detected particles above the GZK threshold, casting doubt on our current understanding of cosmic ray propagation.
- There is no confirmed astrophysical mechanism capable of accelerating particles to $> 10^{20}$ eV.

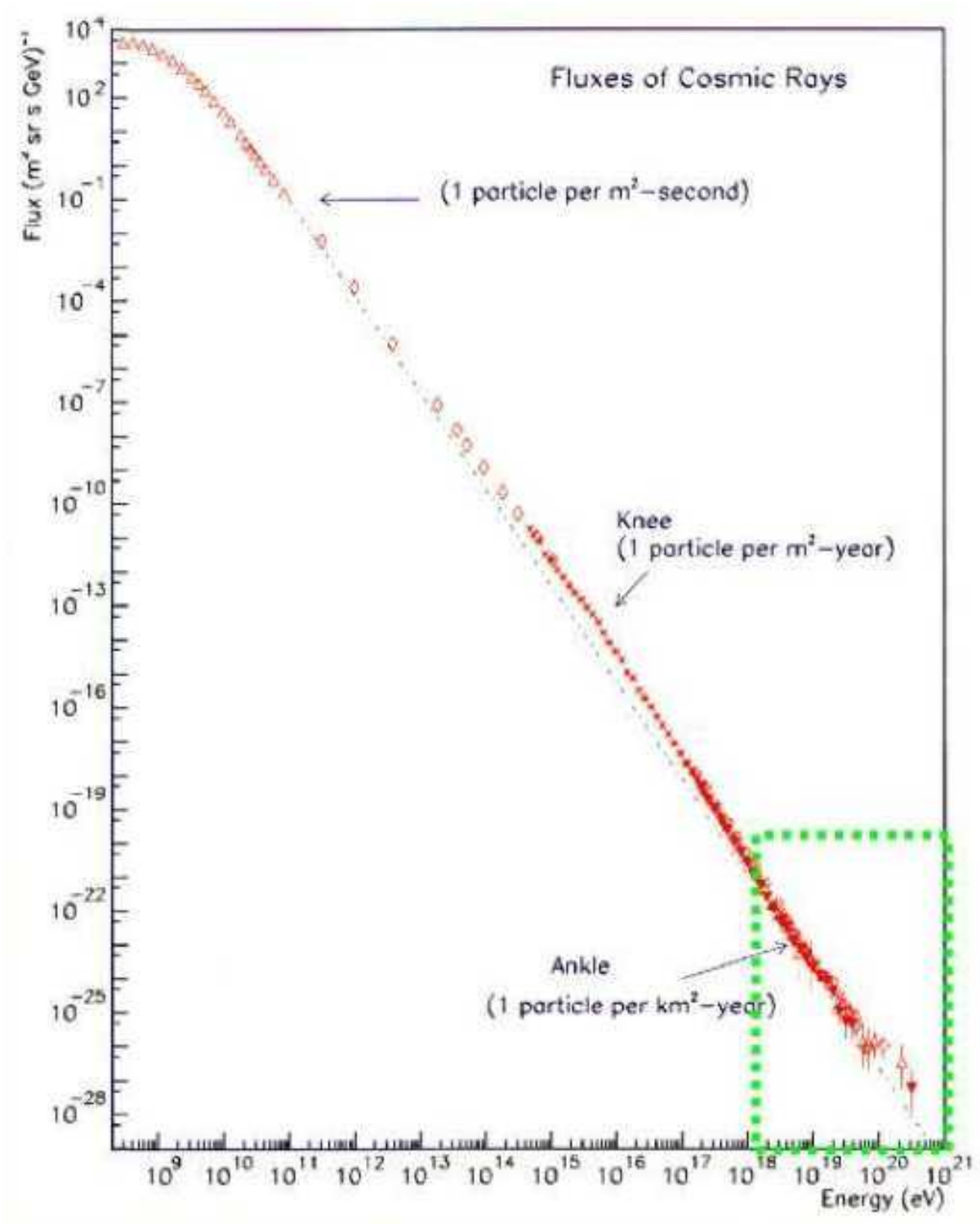

Figure 4.2: Energy spectrum of cosmic rays with possible sources and spectral features.

Chapter 5

Cosmic Rays and Their Detection Methods

5.1 Detection of Primary Cosmic Rays

To observe primary cosmic rays before they undergo any interactions with Earth's atmosphere, specialized instruments must be placed above the atmospheric layer—either on high-altitude balloons or satellites in space. These methods allow for direct detection, providing unaltered information about the energy, charge, and composition of cosmic rays.

5.1.1 Balloon-borne Experiments

Instruments are carried to the stratosphere ($\sim$40 km) via manned or unmanned balloons. Victor Hess, the physicist who discovered cosmic rays, flew a manned hot air balloon for their study. Another example is BESS (Balloon-borne Experiment with a Superconducting Spectrometer).

5.1.2 Satellite-Based Detectors

Detectors and instruments are mounted on artificial satellites and operate in orbit by detecting cosmic rays directly. The AMS-02 (Alpha Magnetic Spectrometer) mounted on the ISS is the most prominent example of such a detector.

The AMS can detect a variety of particles such as electrons, alpha and beta particles, muons, nuclei of heavier elements, etc. It has special sensors that detect antimatter particles as well. By gathering comprehensive data of energies, masses, momenta, fluxes, charges, etc. AMS seeks to unravel profound mysteries, including the potential existence of primordial antimatter from the early universe, indirect evidence of dark matter through anomalies in cosmic ray spectra, and the presence of any exotic forms of matter.

5.2 Detection of Secondary Cosmic Rays

When primary cosmic rays—high-energy particles originating from outer space—enter Earth's atmosphere, they collide with atmospheric nuclei and produce a cascade of secondary particles known as an extensive air shower. These secondary cosmic rays can be detected at the Earth's surface using ground-based observatories.

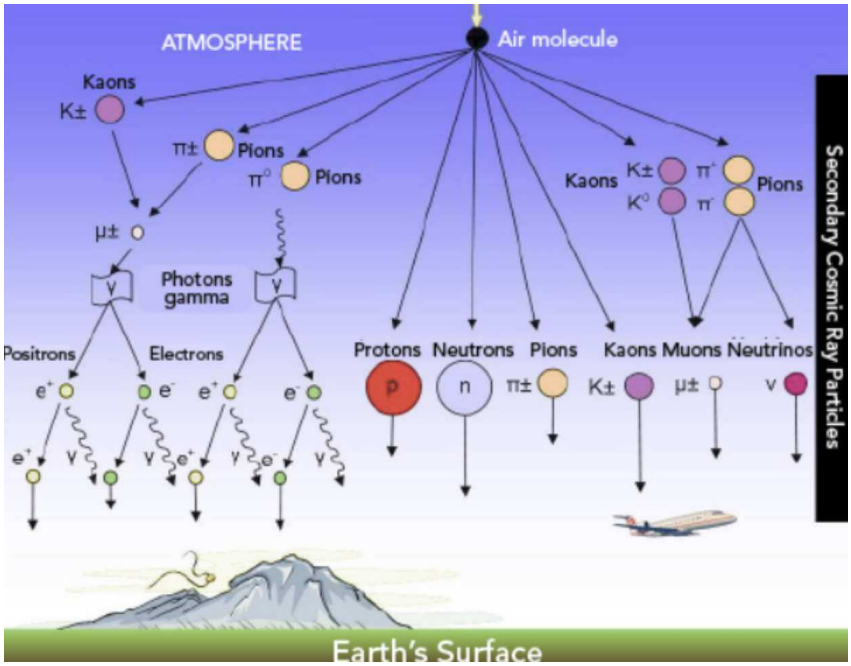

Figure 5.1: Secondary Cosmic Ray Particles

5.3 Detection of UHECRs

When it comes to cosmic ray (CR) detectors, bigger is better. Larger detectors have several advantages:

- They catch more cosmic rays overall.
- They can detect more of the rare events, such as ultra-high-energy cosmic rays (UHECRs) with energies greater than 10^{18} eV, which occur at a rate of only about one per square kilometer per century.
- A larger detection area allows for the observation of bigger particle showers, which result from higher-energy cosmic rays.
- Site selection is also important for optimal detection. For example, the West Desert is an ideal location for fluorescence observations due to its altitude of approximately 4,500 feet, distance from population centers (over 30 miles away), natural shielding from light pollution by surrounding mountains, and excellent visibility—better than 10 miles for 347 days per year

5.4 Detecting an Extensive Air Shower

Two different methods can be used to detect the passage of an extensive air shower: one can look for the particles in the pancake directly, or one can look for the Cherenkov light generated by the particles in the atmosphere. The figure below illustrates both techniques.

The first is an air Cherenkov telescope (ACT). These are large mirrors that focus the Cherenkov light generated by the air

shower onto an array of PMTs, which form an image of the air shower. Properties of the image are used to distinguish between air showers generated by gamma-ray primaries and nuclear primaries. Though very few particles may survive to the ground, the Cherenkov light will reach the ground. Thus, air Cherenkov telescopes can detect lower energy cosmic rays than extensive air shower arrays. However, since they are optical instruments they can only operate on clear moonless nights and they can only view a small piece of the sky at a time.

The second method is to use an EAS array. Figure 5.2 shows an extensive air shower array (EAS array). An EAS array has traditionally been composed of a sparse array of plastic scintillators. The scintillators detect the passage of charged particles that travel through them. They are very inefficient detectors of the gamma rays in the EAS. Since gamma rays outnumber electrons and positrons by a ratio of roughly 4:1 and the scintillator covers less than 1% of the total area of the array, traditional EAS arrays have rather high energy thresholds. Unlike ACTs EAS arrays can operate under all conditions, night or day, and can view the entire overhead sky continuously. By using buried counters they can detect the muons in air showers generated by cosmic-ray nuclei. However, this method of distinguishing between gamma rays and nuclear cosmic rays is not as efficient as the imaging method used by ACTs.

5.5 Pierre Auger Observatory

- Located in Mendoza Province, Argentina
- Contains 1600 water Cherenkov detectors on a 1.5 km grid
- 4 fluorescence eyes—a total of 30 telescopes, each with a 30°

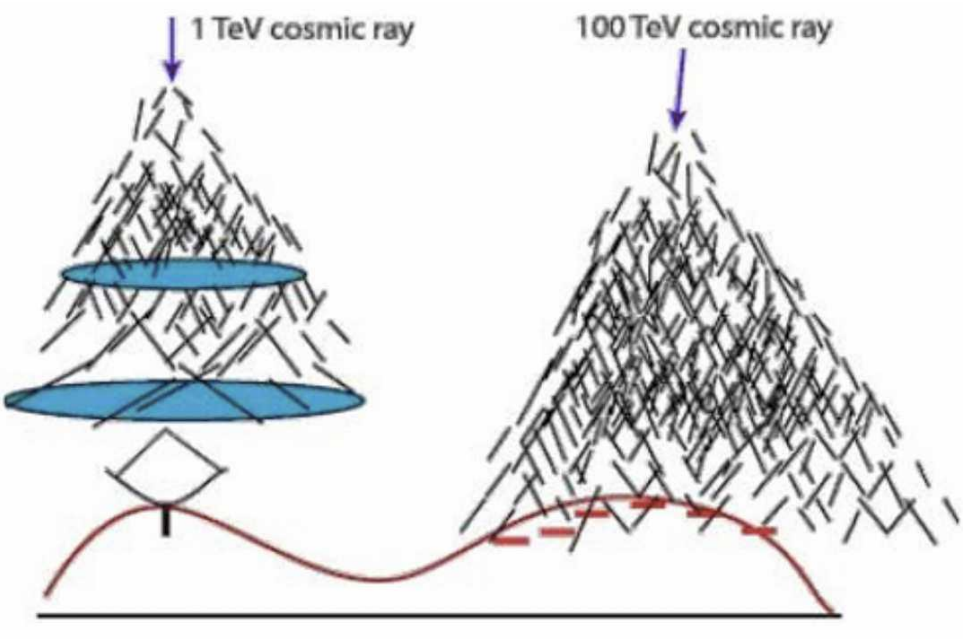

Figure 5.2: An EAS Array

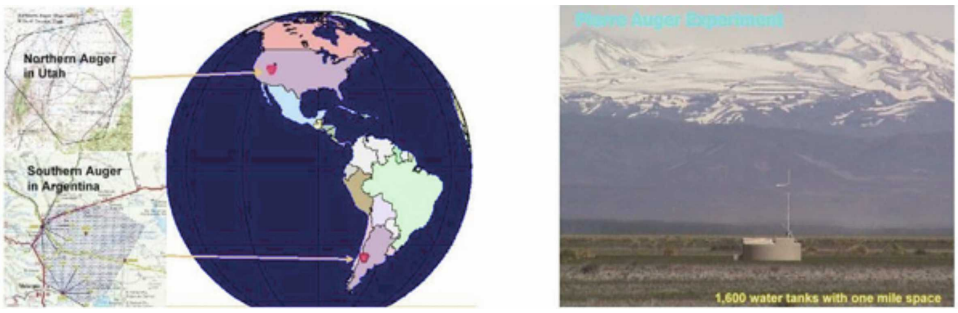

Figure 5.3: Pierre Auger Observatory

$\times$ 30° field of view (FOV)

- Auger will detect the shower in two ways. Twenty four hours a day, an array of over 1600 particle detectors will measure shower particles as they hit the ground, which will allow a reconstruction of the shower providing measures of the original cosmic ray's energy, arrival direction, and mass.
- During clear, moonless nights, the showers will be viewed as they traverse the atmosphere. The passage of the showers will cause the atmosphere to fluoresce, and the faint UV light is detected by arrays of large mirrors equipped with fast photomultiplier image arrays

Chapter 6

Cosmic Rays and Associated Real Life Phenomena

6.1 Air Fluorescence

The passage of charged particles in an extensive air shower through the atmosphere results in the ionization and excitation of the gas molecules (mostly nitrogen). Some of this excitation energy is emitted in the form of visible and UV radiation. This is luminescence, but is referred to as air Fluorescence.

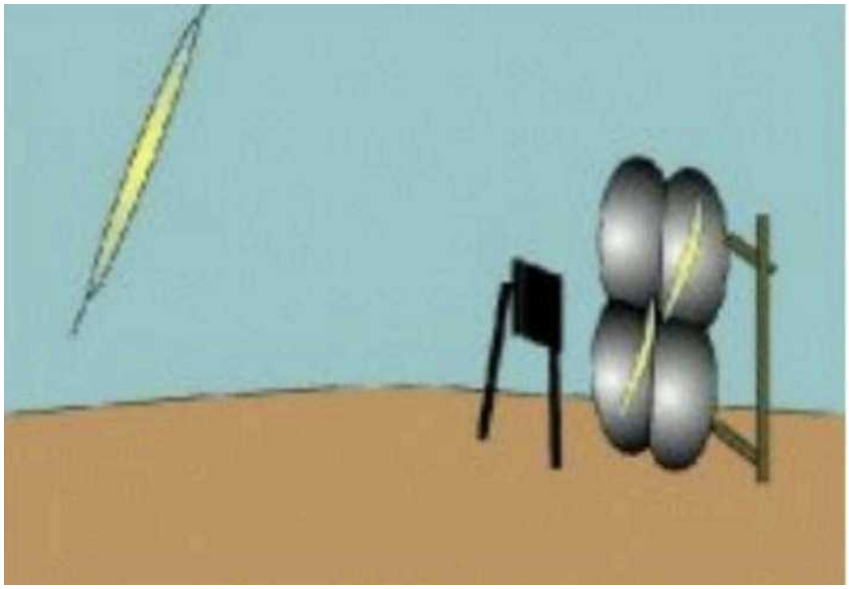

Figure 6.1: Fluorescence Air Shower Detector

This figure shows a schematic of a fluorescence air shower detector. The scintillation light is collected using a lens or a mirror and imaged onto a camera located at the focal plane. The camera pixelizes the image and records the time of arrival of light along with the amount of light collected at each pixel element. This technique can be made to work on clear, moonless nights, using very fast camera elements to record light flashes of a few microseconds in duration.

Many charged particles are expelled from a nuclear explosion, and these particles will also produce scintillation light as they pass through the air. The amount of light collected can then be used to estimate the total energy released from the device.

6.2 Cosmic rays and the weather

While low-energy cosmic rays such as the solar wind cause ionization in the upper atmosphere, muons cause most of the ionization in the lower atmosphere. When a muon ionizes a gas molecule, it strips away an electron, making that molecule into a positive ion. The electron is soon captured, either by another gas molecule forming it into a negative ion, or it may find an already ionized positive ion and neutralize it (this is called recombination).

There is a balance between ionization and recombination, and so there is a fairly constant density of positive and negative ions in the atmosphere. But there is a difference between the types of molecules that become negative ions and the ones that are positive. On average, the negative ions are more "mobile" than the positive ones, and this results in the fact that there is an electric field in the atmosphere.

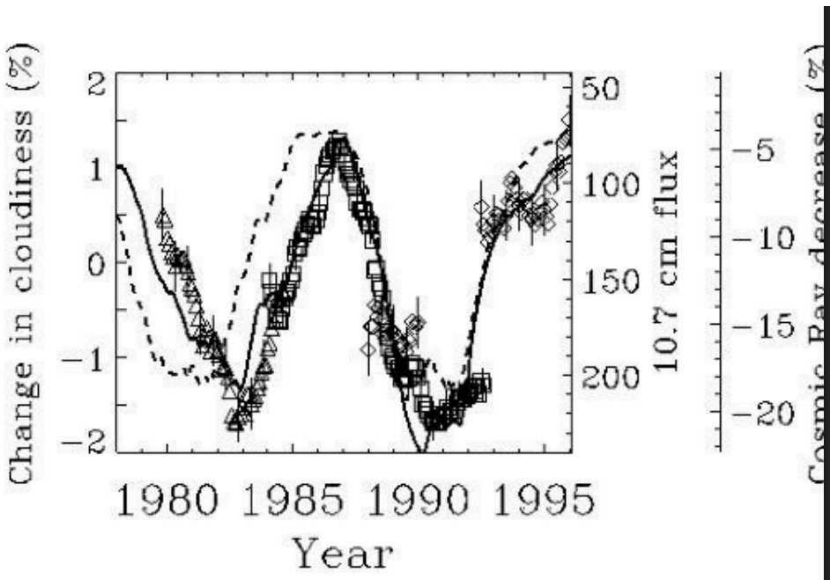

Figure 6.2: Cloudiness is affected by the amount of cosmic rays present

On a normal, quiet day, this electric field is about 100 Volts per meter. When a thunder shower forms, there is an as yet not completely understood mechanism that tends to lift the negative ions up while pushing the positive ones down. This changes the electric field strength to tens of thousands of Volts/meter. When the field strength becomes too high, a discharge occurs: lightning. Clearly, without ionization, thunder and lightning would not happen, so cosmic rays have a direct influence on the types of weather we can have on Earth.

6.3 An Air Show Caused by a Cosmic Ray

When a high-energy cosmic ray enters the atmosphere, it loses its energy via interactions with the nuclei that make up the air. At high energies, these interactions create particles. These new particles go on to create more particles, etc. This multiplication process is known as a particle cascade. This process continues until the average energy per particle drops below about 80 MeV (million electron-volts).

At this point, the interactions lead to the absorption of particles, and the cascade begins to die. This altitude is known as the shower maximum. The particle cascade looks like a pancake of relativistic particles traveling through the atmosphere at the speed of light. Though the number of particles in the pancake may be decreasing, the size of the pancake always grows as the interactions cause the particles to diffuse away from each other. When the pancake reaches the ground, it is roughly 100 meters across and 1-2 meters thick.

If the primary cosmic ray were a photon, the pancake would contain electrons, positrons, and gamma rays. If the primary cosmic ray were a nucleus, the pancake will also contain muons, neutrinos, and hadrons (protons, neutrons, and pions). The number of particles left in the pancake depends upon the energy of the primary cosmic ray, the observation altitude, and fluctuations in the development of the shower. This particle pancake is known as an extensive air shower (or simply an air shower).

6.4 Van Allen Radiation Belts

The Van Allen radiation belts were first observed by the satellite Explorer I in 1958, and their existence was shortly confirmed by Explorer 111 and Sputnik 111 observations. Professor James Van Allen had conducted both experiments on Explorers I and I11 and determined that the observed data indicated the existence of charged particles trapped by the magnetic field.

Over the years, the Van Allen belt has been mapped and refinements have been made in the various zones until finally the picture of an inner and outer zone emerged with particles of energies listed in Table I. Table I is given in the B-L coordinate system, where B is the magnitude of the magnetic induction, and L is the equatorial distance to the dipole field line about which the particles are spiraling. In addition to the naturally occurring radiation zones, high-altitude nuclear explosions have ejected high-energy particles that distort the existing zones.

TABLE 1
VAN ALLEN RADIATION BELT

Heart of Inner Zone ($L \sim 1.4$, $B \cong 0.12$, alt = 3600 km)

Particle	Energy	Flux
Protons	($E > 30$ Mev)	$\sim 3 \times 10^4/cm^2$ sec
Electrons	($E > 600$ Kev)	$\sim 2 \times 10^6/cm^2$ sec
Electrons	($E > 40$ Kev)	$\sim 10^8/cm^2$ sec

Heart of Outer Zone ($L \sim 3.5$, alt $\approx$ 25,000 km)

Electrons	($E > 40$ Kev)	$\sim 10^7/cm^2$ sec
Electrons	($1.5 < E < 5$ Mev)	$\sim 10^4/cm^2$ sec
Protons	($0.1 < E < 5$ Mev)	$\sim 10^8/cm^2$ sec
Protons	($E > 1$ Mev)	$\sim 10^7/cm^2$ sec
Protons	($E > 75$ Mev)	$\sim 0.1/cm^2$ sec

Figure 6.3: Table 1

Fortunately, however, the artificially created belts decay rather rapidly in the outer zones, leaving a more lasting nucleus of high energy particles contained within the limits of the natural radiation zone. It has been found that vehicles in a relatively low circular earth orbit (200-600 km) will receive an insignificant amount of radiation from the Van Allen zones; however, a vehicle with an eccentric orbit or one that has a relatively high circular orbit receives a much higher flux.

For example, a satellite in a synchronous orbit over the equator will be very close to the center of the outer Van Allen zone. Methods are now under development to determine the optimum trajectories (in terms of dose rates) to be used for various mission profiles. If this method proves successful, the mission may be made more complicated due to the specification of a path to be followed through the Van Allen zones.

The Van Allen zones vary diurnally as the magnetosphere. Since on the sunward side of the Earth the magnetosphere is flattened and condensed, the particles which are trapped by the magnetic lines of force are also flattened. At the nadir, however, the magnetosphere is elongated; therefore, the zones of trapped particles are also stretched. It has been discovered that the boundary of the magnetosphere itself contains a great number of charged particles, apparently due to the flow of the solar wind. There have been a number of theories proposed regarding how the Van Allen belts are maintained and how they lose particles. It has been fairly well established that protons are lost to the belts by their interaction with atmospheric constituents.

TABLE 2

RANGES OF PROTONS IN ALUMINUM

Energy (Mev)	Range (gm/cm^2)
10^2	10.5
10^1	1.7×10^{-1}
10^0	3.5×10^{-3}

Figure 6.4: Table 2

Table 2 shows the range that protons have in aluminum. Electrons in the Van Allen belts are probably lost by scattering due to coulomb forces. Several mechanisms have been investigated to determine how the particles are maintained in the belts.

One theory suggests that solar particles may be able to enter the magnetosphere at the polar regions. Such a theory could be acceptable for the outer belt, but the inner belt requires a different explanation. One possibility is that the inner belt is due to the decay of neutrons, but these may only account for the relatively high energy particles. Since the atmospheric density in the exosphere varies markedly with the solar cycle, it should not be surprising to find the particle flux varying inversely with the solar cycle. The Van Allen zones should be of considerable consequence as a radiation hazard to space vehicles.

6.5 Galactic Cosmic Radiation

The radiation with the highest energy per particle encountered in outer space will undoubtedly be the galactic cosmic radiation. Since the flux of these particles is relatively low, the radiation problem will not be as significant as for particles with lower energies and higher flux. The energies of these particles will usually exceed one billion electron volts (1 Bev) and, as a result, may produce secondaries which will be of more concern than the primary radiation itself. Galactic cosmic radiation exhibits a tendency to vary inversely with the solar cycle. This has been attributed to the solar magnetic field lines, which are carried out from the sun farther during higher solar activity periods.

Since the cosmic ray particles are charged, they are deflected by these magnetic lines of force. As the solar activity period decreases, the "interplanetary lines of magnetic force" become weaker, and the resulting deflection of particles becomes less. Thus, fewer particles are excluded from the solar system.

A variation very similar to this is the 27-day variation with the solar cycle. This is due to the reappearance of sunspots that have long lines. These interplanetary magnetic lines of force exhibit variations with the sunspot groups. Since the mean rotational period of the sunspot region is approximately twenty-seven days, the 27-day period exhibited by the cosmic rays is considered to be a direct result. The final variation noted in the flux of cosmic rays reaching the Earth is known as the Forbush decrease. The Forbush decrease is a significant decrease in the flux of cosmic rays incident on the Earth following a solar flare. A decrease of approximately 30% of the flux has been noted, and the recovery time following the decrease is usually from one to two days. This phenomenon is considered to be caused by the ejection of a vast plasma cloud. This cloud, in turn, carries 5 magnetic lines of force away from the surface of the sun.

When the cloud reaches the earth, the cosmic rays suddenly decrease due to the presence of the magnetic lines of force. At about the same time, the beginning of a magnetic storm takes place as well as the other associated geomagnetic disturbances. Particles reaching the earth will penetrate the magnetic field to a certain depth depending upon the rigidity, R, exhibited by the particles.

TABLE 3
COMPOSITION OF GALACTIC COSMIC PARTICLES

Particles	Flux (R ≧ 4.5 bv)	Percent
Protons	~ .77/cm^2-sec	~ 84%
Alpha Particles	~ .11/cm^2-sec	~ 14%
Carbon, Nitrogen, Oxygen*	~ .009/cm^2-sec	~ 1%
Z > 10	~ .002/cm^2-sec	~ 0.25%
Gamma Radiation and Electrons**	---	~ 1%

Figure 6.5: Table 3

$$R = \frac{pc}{Ze}$$

Rigidity is simply the ratio of the particle's momentum to its charge, where p is the momentum (in units of Bev/c), c is the velocity of light, Z is the atomic number, e is the unit charge, and the resulting R is in billion volts. If we examine the formula and assume a uniform velocity for particles of any mass, we see that R increases as we go up the atomic scale, since the mass increases faster than does Ze. Then, higher mass particles will penetrate deeper into the magnetic field of the earth than will the lower mass particles.

A generalised table of composition for galactic cosmic radiation is found in Table 3. The energy range for these particles ranges from a few MeV up to at least 10^{12} MeV, with the average energy in the vicinity of $4 * 10^3$ Mev. Despite the high energies that the galactic cosmic rays exhibit, there will be little biological hazard during short-term missions due to this radiation. On longer missions the situation may change due to the constant accumulation of radiation.

6.6 Solar Wind

In interplanetary space, the surrounding plasma will have some kinetic velocity due to the high temperatures in the corona. At present, there is some evidence to suggest that the corona exhibits a "breathing" effect which varies directly with the eleven-year solar cycle period. This seems to be borne out when one observes the density and velocity variations of the plasma flow during minimum and maximum sunspot activity. During the minimum sunspot activity at the Earth's distance from the sun, the mean density of the solar wind is approximately 10^2 particles per cm^3 traveling at a velocity of 500 kilometers per second. This results in an average particle flux of about $5 * 10^9$ particles/cm^2 sec.

At sunspot maximum the density of particles is expected to increase to approximately 10^3 particles per cm^3, with a velocity in the vicinity of 1500 kilometers per second. This results in a particle flux at the earth's orbit of about $1.5 * 10^{12}$ particles/cm^2 sec. The kinetic temperature in the earth's vicinity is approximately $220{,}000^0$ C. However, this will have a very small effect on the heating of vehicles when one considers that the solar radiation flux will amount to about $1.4 * 10^6$ ergs/cm^2 sec. (September-December 1962) data obtained by a plasma probe, plasma energy is approximately $4.4 * 10^{-9}$ ergs/cm^2.

From an analysis of Mariner II, the solar wind is considered to encompass the Earth's magnetosphere and to flow around the outer boundaries much like the wake of a bullet as it passes through air. The magnetosphere is thus flattened on

the sunward side of the earth and elongated on the dark side. Although the flux of particles in the solar wind is high, their energies are relatively low. For this reason, It is expected that the biological radiation hazard behind a small amount of shielding will be insignificant.

6.7 Solar Flares

Solar flares will undoubtedly be the source of radiation that should concern us most during interplanetary travel. The "great solar bursts" or type 3+ flares emit particles with near-relativistic velocities. These particles have energies comparable to the galactic cosmic rays, but their flux is much greater. Solar flares are associated with the dark spots noted on the photosphere of the sun. The dark spots are local magnetic fields of great intensity. These high magnetic fields inhibit the outward flow of the hot gases from within, and thus cause cooler and darker patches on the 7 photosphere of the sun. If these areas "collapse" due to the buildup of strong perturbing fields by the ionized gas flowing around the sunspots, then great volumes of ionized gases are spewed out into the chromosphere. This phenomenon is known as the solar flare.

Much of the data presently available, which tells the story of the solar flare, has been accumulated by studies of the various radio wave emissions accompanying the solar flare. The refractive index of an ionized medium is based upon the physical characteristics of the medium itself. The refractive index, μ, of a medium (containing N number of particles with charge e and mass m) to a wave with frequency f is

$$\mu^2 = 1 - \frac{N\ e^2}{\pi\ \epsilon_0\ mf^2}\ .$$

Assuming that electrons are the particles affecting the refractive index the most, we may substitute the mass and charge of the electron for m and e. The point at which μ^2=0 is the point at which the radio waves will be refracted.

This means, that (assuming N increases as we approach the sun) any frequency, f, must have originated at some distance from the sun equal to or greater than the distance of which $f = 9 * 10^{-3}\sqrt{N}$. For this reason frequencies ranging from about 300 to 30,000 megacycles/sec are assumed to originate in the chromosphere, whereas lower frequencies are assumed to originate in the corona. As the frequency becomes lower, it must have originated at greater and greater distances from the sun. Figure 1 illustrates when the specific radio bursts occur and in what frequency range during a solar flare. Table 4 is a summary of the various characteristics of radio emissions from the sun .

The flux and energies of the emitted particles are of primary concern when considering the effects of solar flares. It is impossible to make any specific statement as to the flux of particles at the earth from any flare. This is because the flux of particles of a particular energy depends not only upon the characteristics of the flare itself, but also upon the location of the flare on the surface of the sun. In the same sense, the flux of particles is dependent upon the location of the earth

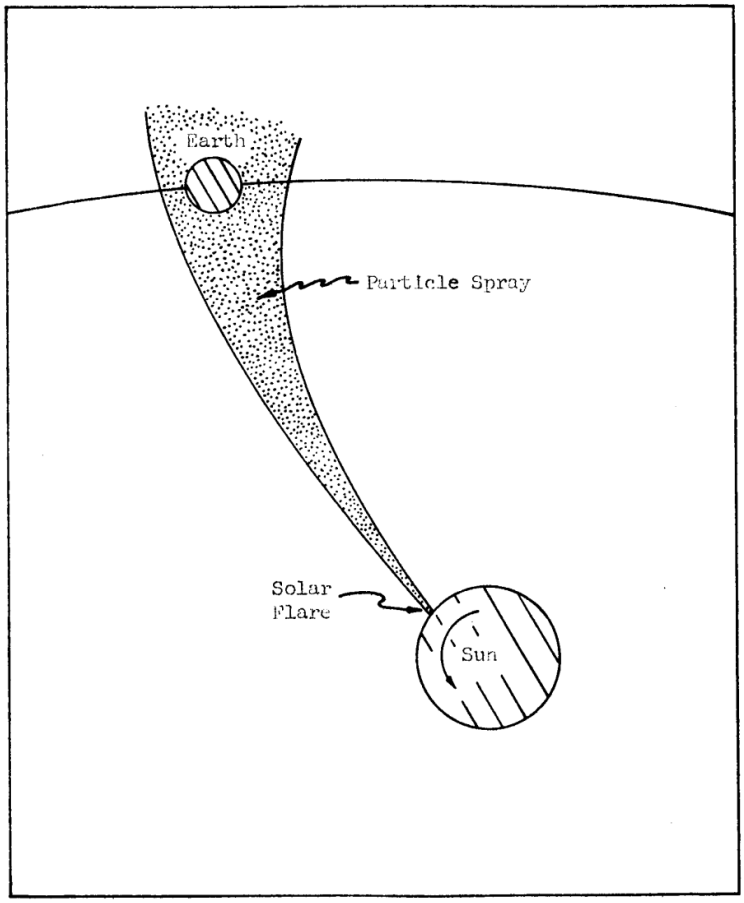

Figure 2. Path Along Which Particles From the Sun Following A Solar Flare Travel, As Seen From Above the Plane of the Ecliptic

as it orbits around the sun. Anyone who has ever watched a rotating lawn sprinkler can visualise the path which solar particles take as they erupt from the sun (Fig. 2). To an observer in the path of the particles, however, the flux would appear to be traveling in a straight line from the sun. Table 5 gives the ranges over which the magnitude of the solar flares may be expected to extend. The wide range is necessitated by the variables which may exist.

TABLE 4

CHARACTERISTICS OF SOLAR NOISE

Type	Identifying Characteristics	Source Characteristics	Frequency Characteristics
I	Noise storms usually lasting from hours to days; or bursts of ~ 1 second duration.	Assumed to be of a non-thermal origin, associated with sunspots, "R centers," and sometimes flares.	Less than ~ 250 Mc/sec with bandwidth 1-10 Mc/sec for bursts and 10-100 Mc/sec for continuum. The intensity at 100 Mc/sec 10^{-21} - 10^{-19} $\frac{\text{watts}}{\text{m}^2\ \text{c/s}}$.
II	Bursts with slow drift of ~ -0.3 Mc/sec^2 lasting from 5-10 minutes.	Source is due to plasma oscillations associated with flares. Occurrence begins about 7 minutes after flare. The source moves outward at ~ 1000 km/sec.	Mainly less than 150 Mc/sec with the bandwidth of about 2×10^{-1} of the observed frequency. Intensity at 100 Mc/sec is usually 10^{-20} to 10^{-19} $\frac{\text{watts}}{\text{m}^2\text{(c/sec)}}$
III	Bursts with fast drift of ~ 30 Mc/sec^2 lasting singly 3-10 sec or in groups of 1-5 minutes.	Assumed to be associated with plasma oscillation associated 50-60% of the time with flares. The source has an outward velocity of ~ 10^5 km/sec.	Ranges from > 4000 Mc/sec to < 10 Mc/sec with a bandwidth almost equal to the frequency. The intensity usually is less than 10^{-20} $\frac{\text{watts}}{\text{m}^2\text{(c/sec)}}$.

TABLE 4 (Cont'd)

Type	Identifying Characteristics	Source Characteristics	Frequency Characteristics
IV	Smooth continuum lasting from minutes to hours.	Source is due to synchrotron radiation. Occurring 70-80% of the time with flares at ~ 15 minutes after start. Initial source velocity ranges from $1\text{-}5 \times 10^3$ km/sec for about 10 minutes and then source becomes stationary.	Cover the complete radio band but vary from burst to burst. The bandwidth is frequently several octaves with intensities from 10^{-20} to 10^{-19} $\frac{\text{watts}}{\text{m}^2\text{(c/sec)}}$.
V	Smooth continuum lasting from 1-2 minutes.	Synchrotron radiation occurring before the maximum of solar flares. The velocity of the source is ~ 5×10^3 km/sec.	Frequencies less than 200 Mc/sec with a bandwidth of several Mc/sec at 50-100 Mc/sec. Intensities 10^{-20} to 10^{-19} $\frac{\text{watts}}{\text{m}^2\text{(c/sec)}}$.
Microwave	Continuum and bursts lasting 0.5 to 20 minutes.	Assumed to be of synchrotron and possibly thermal origin associated about 80% of the time with flares.	The frequency range is ~ 1000-20,000 Mc/sec with a bandwidth of several octaves. The intensity is usually ~ 5×10^{-22} to 5×10^{-20} $\frac{\text{watts}}{\text{m}^2\text{(c/sec)}}$ at 3000 Mc/sec.

6.8 Spectral Radiation

Of all the radiation hazards which will be encountered in space, the effects of spectral irradiation are the most difficult to analyse at the present time. This is true because of the difficulty in studying the solar photon flux in this most important range below 3000 A^0. Since radiation of wavelengths less than 3000 A^0 is strongly absorbed by our atmosphere, earth-bound studies in this range are mostly hypothetical. Artificial sources of photon flux in the X-ray and γ-ray range have been studied and may inform us as to the hazards which may be encountered.

TABLE 5 (Ref. 6)

PARTICLE RADIATION DUE TO SOLAR FLARES

Flux	Range from 3 x 10^3 to 1.2 x 10^4/cm^2 sec-ster distributed isotropically, and containing predominantly H^+ particles.
Energy	Range from ~ 10 Mev to ~ 500 Mev.
Duration	From 10 to 100 hours.
Origin	Associated with class 3 or greater flares, which follow the solar cycle: ~12/yr at solar maximum to ~3/yr at solar minimum
Dose	Depending upon flux and energy ranges from 10^{-3} rad to 10^3 rad.

TABLE 6

Wavelength Å	Percent of solar Electromagnetic Energy
< 2000	0.2
2000 - 3800	7.5
3800 - 7000	41.0
7000 - 10000	22.0
10000 - 20000	23.0
> 20000	6.0

In the region from about 2200 A^0 to 2900 A^0, atmospheric ozone absorbs almost all the photon radiation. From about 9000 A^0 atmospheric oxygen above 75 km absorbs the radiation, and below 900 A many atmospheric constituents share in absorbing radiation .

Table 6 summarizes the percent of solar electromagnetic energy radiated in various wavelength intclrvals. Figure 3 illustrates the wavelength spectrum from the sun, and Figure 4 is a corresponding frequency graph.

The most hazardous region of the electromagnetic spectrum is the short wavelength X-ray range. Fortunately, the most predominant energy region is not in this range. The X- and y-radiations increase as solar flares occur.' The following table lists the X-ray fluxes detected by rocket-borne

TABLE 7

	Date	2-8 Å ergs/cm^2 sec	8-20 Å ergs/cm^2 sec	44-60 Å ergs/cm^2 sec
Background and Bright Surge	7-24-59	1.3×10^{-2}	9×10^{-2}	0.15
Background	8-7-59	0.1×10^{-2}	2.3×10^{-2}	----
Background	8-14-59	0.1×10^{-2}	2.3×10^{-2}	0.075
Background	8-29-59	0.33×10^{-2}	----	0.17
Flare 2+	8-24-59	2.6×10^{-2}	16×10^{-2}	< 0.41
Flare 2+	8-31-59	3×10^{-2}	90×10^{-2}	< 1.8
Flare 2+	9-1-59	$> 8.8 \times 10^{2}$	$> 90 \times 10^{2}$	----

equipment.

From most of the data presently available, it appears that the spectral component of radiation need not be considered. The effects of the electromagnetic radiation on the eyes are apparent.

6.9 Conclusion

From the preceding sections it is apparent that Van Allen and solar flare radiations need be of primary concern during space flight. A long duration earth orbit, as well as an extended extraterrestrial mission, must be adequately protected against the harmful radiations which each will encounter. In the case of an extended earth orbit where the radiation dose may be accumulated over a period of time, the obvious solution is to have the personnel periodically replaced and sensitive instrumentation adequately protected. By a frequent replacement of personnel, the dose will not have time to accumulate to serious proportions. Such an

arrangement would obviously be required for a manned orbiting space station or orbiting laboratory. This might become troublesome to the people working on a specialized problem to which they have become dedicated, or to persons working in intricate areas where several people would have to be trained in one specialized area. Other than these human factors, the problems involved do not appear too difficult.

On an extended extraterrestrial mission, personnel cannot be replaced as they acquire a specific minimal amount of radiation. One solution to this problem might be to fractionate the dose. Assuming complete shiel-ding for the entire vehicle will not in itself be sufficient to cope with any situation, it may be more realistic to provide an area which has sufficient shielding to cope with any radiation hazard. Each member of the crew would be required to spend a certain portion of his time in this area. During solar flares perhaps all members of the crew could remain in this area for a short period of time (about three to four hours). Such an arrangement is obviously to be included for conservation of shielding weight. The engineering problems encountered may be a bit more complicated, but nothing which cannot be overcome. At the present time very little is known of the effects of radiation on the human body, especially the effects which exposure to radiation may impose upon future generations. In addition, sensitive vehicle instrumentation - especially items concerned with the guidance and control'systems and the spacecraft life systems - must be adequately tested to establish limits of radiation exposure so that this equipment may be protected from possible excess.

Chapter 7

Computational Methods

7.1 Objective

Image processing is an integral part of Observational Astronomy, as it is used for refining the raw data collected from telescopes like images of distant galaxies, supernovae, black holes, exoplanets and many more... Through this

task, we aim to apply some of the image processing techniques like filtering, edge detection, contrast enhancement, and geometric transformations — over a set of images of Cats and Dogs.

7.2 Tools Used

- Python
- OpenCV (CV2)
- Pandas
- Numpy
- Matplotlib

7.3 Image into arrays

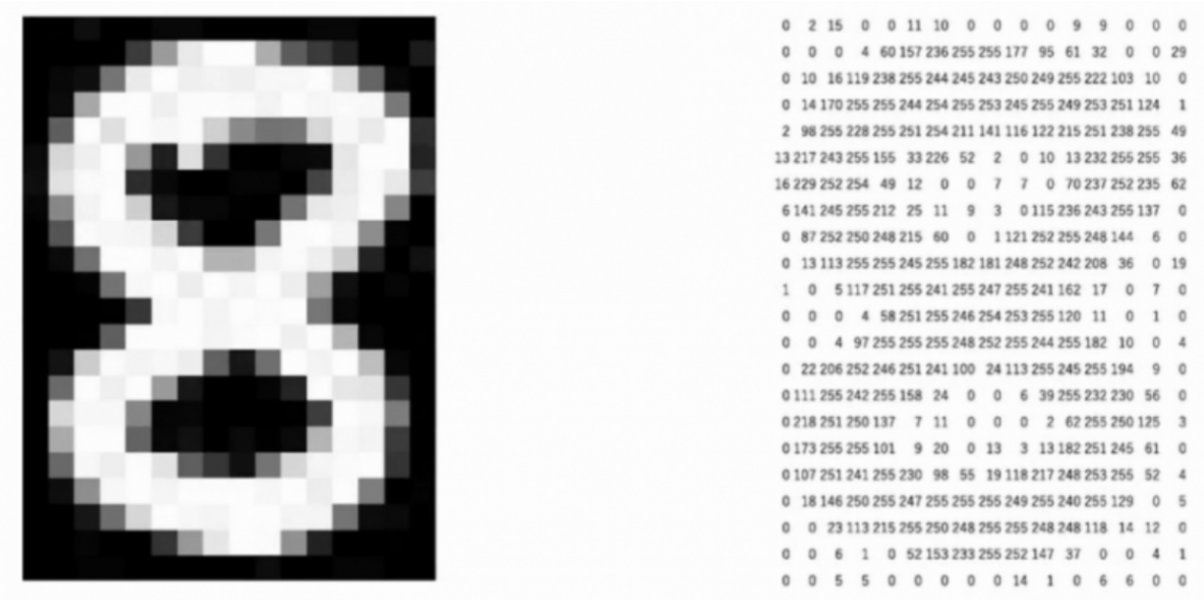

Figure 7.1: BW image into array

An RGB image is composed of three color channels:
Red, Green, and Blue — which correspond to the way human eyes perceive color. Each channel having intensity between 0-255.
Cv2 - reads these channels as BGR and matplotlib reads RGB.
Here's a comparison between image interpreted in OpenCV and image in Matplotlib

7.4 Image Manipulation

7.4.1 Gray scaling

this is the snippet used to convert into a grey image..


```
img_gray = cv2.cvtColor(img, cv2.COLOR_RGB2GRAY)
fig, ax = plt.subplots(figsize=(8, 8))
ax.imshow(img_gray, cmap='Greys')
ax.axis('off')
ax.set_title('Grey Image')
plt.show()
```

Figure 7.2: Grayscaling

7.4.2 Resizing the image

7.4.3 Scaling the image

This snippet scales the images pixels to 25% of what it initially had Say 1000 x 800 pixels, now it has 250 x 200 only

```
img_resize = cv2.resize(img, (100, 200))
fig, ax = plt.subplots(figsize=(8, 8))
ax.imshow(img_resize)
ax.axis('off')
plt.show()
```

```
img_resized = cv2.resize(img, None, fx=0.25, fy=0.25)
fig, ax = plt.subplots(figsize=(8, 8))
ax.imshow(img_resized)
ax.axis('off')
plt.show()
```

7.4.4 Sharpening the image

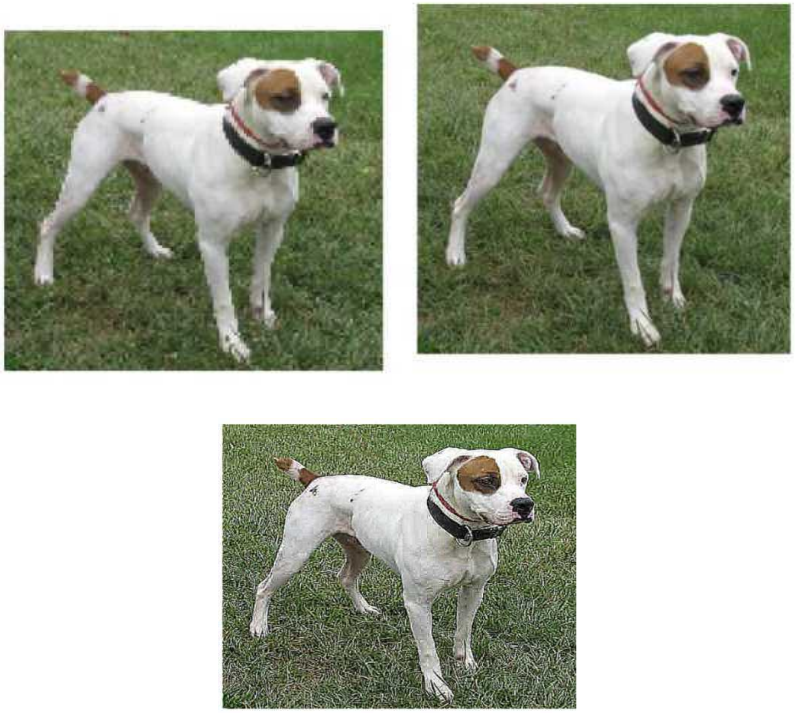

7.4.5 Blurring the image

```
kernel_sharpening = np.array([[-1,-1,-1],
                              [-1,9,-1],
                              [-1,-1,-1]])

sharpened = cv2.filter2D(img, -1, kernel_sharpening)

fig, ax = plt.subplots(figsize=(8, 8))
ax.imshow(sharpened)
ax.axis('off')
ax.set_title('Sharpened Image')
plt.show()
```

```
kernel_3x3 = np.ones((3, 3), np.float32) / 9
blurred = cv2.filter2D(img, -1, kernel_3x3)
fig, ax = plt.subplots(figsize=(8, 8))
ax.imshow(blurred)
ax.axis('off')
ax.set_title('Blurred Image')
plt.show()
```

Chapter 8

Introduction to Cloud Chambers

8.1 Overview of Clouds and Their Role in the Climate System

Clouds play a crucial role in Earth's climate system by regulating the planet's radiation budget. They reflect and scatter incoming solar radiation while absorbing and re-emitting infrared radiation from the Earth's surface. Additionally, clouds are fundamental to the hydrological cycle, as they facilitate precipitation.

The formation of clouds depends on **hygroscopic nuclei** (aerosols), which act as seeds for water vapor condensation. The microphysical properties of clouds—such as droplet size, concentration, and liquid water content—determine their radiative effects. Variations in aerosol composition, humidity, and turbulence influence cloud formation, making it a complex and dynamic process.

8.2 Studying Cloud Processes: Methods and Challenges

Understanding cloud dynamics requires a combination of:

- **Satellite observations** (limited by temporal resolution)
- **Ground-based measurements** (limited by spatial coverage)
- **Model simulations** (helpful but require validation)
- **Laboratory experiments** (controlled conditions for detailed analysis)

Among these, **cloud chambers** provide a unique experimental approach to simulate atmospheric processes under controlled conditions, bridging gaps between theoretical models and real-world observations.

8.3 Evolution of Cloud Chambers

The first cloud chamber was developed by **C.T.R. Wilson in 1911** to study particle tracks, but its potential for cloud physics research was soon recognized. Over time, cloud chambers evolved into sophisticated tools for atmospheric studies:

- **Expansion Cloud Chambers** – Early designs for nucleation studies
- **Continuous Flow Chambers** – Enabled long-duration experiments with aerosols
- **Turbulence-Based Chambers** – Simulated atmospheric mixing effects
- **Wind Tunnels** – Studied cloud dynamics under varying airflow conditions

Modern cloud chambers, such as the **Manchester Ice Cloud Chamber**, have been used to investigate ice particle scattering, droplet nucleation, and turbulence effects.

8.4 Key Applications of Cloud Chambers

Cloud chambers help researchers study:

- **Nucleation Mechanisms** – How aerosols trigger droplet formation
- **Turbulence Effects** – Impact on droplet distribution and precipitation
- **Light Attenuation** – How clouds scatter and absorb radiation
- **Artificial Precipitation** – Techniques like laser-induced condensation (as an alternative to traditional cloud seeding with silver iodide)

8.5 Objectives of Cloud Chamber Experiments

The primary goals of experimental studies using cloud chambers include:

- Observing **temperature gradients** and their effect on droplet formation
- Analyzing **droplet size distribution** under varying turbulence conditions
- Measuring **light attenuation** due to changing droplet concentrations
- Validating theoretical models with empirical data

8.6 Significance in Climate and Weather Research

Cloud chambers provide critical insights into:

- **Cloud-Climate Feedback Mechanisms** – How clouds influence global warming
- **Precipitation Efficiency** – Factors affecting rain and snowfall
- **Aerosol-Cloud Interactions** – The role of pollution in altering cloud properties

By replicating atmospheric conditions in a controlled setting, cloud chambers enhance our understanding of cloud microphysics, helping improve weather forecasting and climate models.

8.7 Future Prospects

Advancements in cloud chamber technology, such as **laser-based condensation techniques** and high-resolution sensors, will further refine our ability to simulate real-world cloud processes. Continued experimentation will address unresolved questions about cloud dynamics, turbulence effects, and aerosol-cloud interactions, contributing to more accurate climate predictions.

This chapter sets the foundation for understanding how cloud chambers serve as vital tools in atmospheric science, enabling researchers to explore complex cloud processes in a controlled laboratory environment.

Chapter 9

Types of Cloud Chambers

9.1 Diffusion Cloud Chambers

Diffusion cloud chambers represent a significant evolution from expansion-type chambers, enabling continuous operation without mechanical pressure changes. This section details their operating principles, design characteristics, and experimental applications.

9.1.1 Operating Principle

Diffusion chambers create supersaturated vapor through vertical temperature stratification:

- **Cold base**: Maintained at $-20°C$ to $-40°C$ (liquid nitrogen/Peltier cooling)
- **Warm top**: Ambient temperature ($\sim 20°C$)
- **Alcohol reservoir**: Ethanol/isopropanol-saturated felt liner

Alcohol vapor diffusing downward encounters decreasing temperatures, reaching supersaturation ($S = P_v/P_{\text{sat}}(T) > 1$) near the cold plate. Charged particles ionize vapor molecules, creating nucleation sites for visible droplet tracks (10-100 μm).

Figure 9.1: Temperature gradient and vapor diffusion in diffusion cloud chamber

9.1.2 Key Components

Table 9.1: Design Components of Diffusion Chambers

Component	Function
Metal Base Plate	High-thermal-conductivity (Cu/Al) cold surface
Transparent Enclosure	Glass/acrylic walls for observation
Felt Liner	Alcohol reservoir at chamber top
Source Port	Insertion point for radioactive materials
HV Electrode	Enhances track density (5-15 kV)
Insulation Layer	Maintains temperature gradient

9.1.3 Operational Characteristics

- **Sensitive Volume**: Typically 10×10×5 cm (height-dependent)
- **Temperature Gradient**: 10-20°C/cm vertical stratification
- **Startup Time**: 5-10 minutes for vapor equilibration
- **Operation Duration**: 2-4 hours per liquid nitrogen fill
- **Track Lifetime**: 0.1-1 second visibility window

9.1.4 Advantages over Expansion Chambers

- Continuous operation without expansion cycles
- No moving parts or pressure systems
- Lower maintenance requirements
- Atmospheric pressure operation
- Real-time particle tracking capability

9.1.5 Experimental Applications

Diffusion chambers enable investigations of:

- Particle track curvature under magnetic fields ($p = qBR$)
- Radon detection via alpha decay counting
- Rutherford-style scattering using metal foils
- Energy loss studies with material shielding
- Nucleation thresholds via corona discharge

9.2 Atmospheric Cloud Chambers

Atmospheric cloud chambers are specialized laboratory systems designed to simulate cloud microphysical processes under controlled conditions. Unlike particle detection chambers, these focus on replicating atmospheric phenomena such as droplet formation, precipitation mechanisms, and aerosol-cloud interactions. The chamber described by Goti et al. exemplifies this category, enabling experimental studies of turbulence effects on cloud dynamics.

9.2.1 Design and Construction

- **Dimensions**: 0.55 m × 0.6 m × 1 m acrylic enclosure (5 mm thickness)
- **Temperature control**: Dry ice cooling system achieving -8°C at base (simulating mid-level clouds)
- **Humidity system**: Steam injection at 0.8 m height via boiler (70°C water vapor source)
- **Turbulence generation**: Variable-speed fan (2.8–14.4 m/s) for controlled mixing

- **Observation ports**: Laser windows and optical access points

9.2.2 Instrumentation

Table 9.2: Measurement Systems in Atmospheric Cloud Chambers

Instrument	Function
Hygrometer	Temperature/humidity profiling (±0.1°C, -40–100°C)
He-Ne Laser (632.8 nm)	Light attenuation studies
Lux Meter	Scattered light intensity measurement
DSLR Camera (18 MP)	Droplet imaging and size analysis
ImageJ Software	Droplet distribution quantification

9.2.3 Key Experimental Capabilities

- **Turbulence-droplet interactions**: Quantify collision-coalescence processes
- **Light attenuation studies**: Measure scattering dependence on droplet concentration
- **Temperature-humidity profiling**: Vertical gradient analysis (0–80 cm height)
- **Droplet size distribution**: Gaussian distribution fitting under varying turbulence

9.2.4 Characteristic Findings

Temperature-Humidity Profiles

- Near-linear temperature gradient from -6°C (base) to 23°C (top)
- Humidity $\geq$99% throughout chamber during operation

- Gradient steepness inversely proportional to turbulence:

$$\Delta T_{\text{low}} = 29°\text{C}\,(2.8\,\text{m/s})$$
$$\Delta T_{\text{high}} = 27°\text{C}\,(14.4\,\text{m/s})$$

Light Attenuation

Turbulence reduces scattering efficiency:

Table 9.3: Turbulence Effects on Light Transmission

Turbulence (m/s)	**Luminosity (lux)**	**Attenuation (%)**
2.8	70	76.67
7.2	103	65.67
14.4	125	58.34

Droplet Size Distribution

- Gaussian distribution confirmed for all turbulence regimes
- Mean droplet size increases with turbulence:

$$r_{\text{low}} = 3.39 \pm 2.83\,\text{mm}$$
$$r_{\text{high}} = 3.91 \pm 3.18\,\text{mm}$$

- Enhanced collision-coalescence at higher turbulence

Figure 9.2: Droplet size distribution at varying turbulence intensities (Goti et al.)

9.2.5 Applications and Limitations

Research Applications

- Precipitation efficiency studies
- Aerosol-cloud interaction mechanisms Cloud radiative properties analysis
- Turbulence-microphysics parameterization

9.3 TRONIC Cloud Chamber

The TRONIC cloud chamber represents an innovative refrigeration-based approach to particle detection, addressing limitations of traditional Wilson chambers through engineered cooling systems. Developed by Lakshminarayana (2014), this design eliminates dependency on dry ice while enabling operation in isolated field conditions ideal for cosmic ray studies.

9.3.1 Design Innovations

- **Compact dimensions**: 510 mm × 180 mm × 700 mm glass chamber
- **Refrigeration system**: Copper coils with anhydrous ammonia coolant (NH_3 aqueous solution)
- **Thermal management**: Aluminum heat sink plate + condenser with cooling fan
- **Cooling capacity**: Achieves -16°C (phase transition threshold)
- **Power system**: 12V DC pump for coolant circulation

Figure 9.3: TRONIC chamber's refrigeration schematic (Lakshminarayana, 2014)

9.3.2 Operating Principle

The system creates supersaturation through thermodynamic cooling:

1. Coolant circulates through copper coils beneath aluminum plate
2. Heat transfers from ethanol-filled chamber to coolant

3. Vertical temperature gradient established (2°C to -16°C)
4. Cosmic rays ionize vapor, forming visible tracks

The cooling profile follows:

$$\frac{dT}{dt} < 0 \quad \text{(until -16°C)} \rightarrow \quad \frac{dT}{dt} \approx 0 \quad \text{(phase transition)}$$

9.3.3 Particle Identification

Table 9.4: Track Characteristics in TRONIC Chamber

Track Feature	**Particle Identification**
Thick, short trails	High-energy alpha particles
Long, thin trails	Muons
Thick, extended trails	Beta particles
Branched trajectories	Delta rays (Rutherford scattering)

9.3.4 Performance Advantages

Over Dry Ice Chambers

- Eliminates rapid sublimation issues
- Maintains stable temperatures >4 hours
- Eco-friendly (no CO_2 release)

Over Electromagnetic Chambers

- No wire-induced particle interference
- Operates without continuous grid power
- Reduced experimental noise

9.3.5 Field Deployment Capabilities

- Portable design for high-altitude cosmic ray studies
- Optimal operation at 4115m altitude (validated)
- Magnetic curvature analysis of low-momentum muons
- Energy loss measurements via track radius variation

9.3.6 Technical Significance

This refrigeration-based approach demonstrates:

- Viable alternative to hazardous coolants
- Scalable miniaturization for field studies
- Sustainable operation in power-constrained environments
- Extended observation windows for rare cosmic events

9.4 Expansion Cloud Chambers

The expansion cloud chamber, pioneered by C.T.R. Wilson in 1911, represents the original design for visualizing ionizing radiation through controlled adiabatic expansion. As documented in the Mound Laboratory report (1949), this chamber type enables precise study of particle interactions through vapor trail formation.

9.4.1 Operating Principle

- **Supersaturation mechanism**: Adiabatic expansion reduces pressure, causing saturated vapor to become supersaturated

- **Ion visualization**: Charged particles create ion pairs that act as condensation nuclei
- **Track formation**: Vapor condenses into visible droplets along particle paths (0.1-1 second visibility)
- **Cyclic operation**: 15-20 second cycles for droplet clearance and equilibrium restoration

9.4.2 Core Components

Table 9.5: Essential Elements of Expansion Chambers

Component	**Function**
Glass enclosure	Visible track observation
Rubber diaphragm	Pressure control mechanism
Circular glass rim	Gas/vapor containment
Magnetic valves	Synchronized pressure control
Colloidal graphite ring	Ion sweeping electrode
Flashing illumination	High-intensity track lighting (7000K)

9.4.3 Key Technical Parameters

- **Expansion ratio**: 1.2-1.4 (adjustable via rubber ring thickness)
- **Sensitive volume**: Typically 30-40 cm diameter $\times$ 30 cm depth
- **Gas media**: Hydrogen, helium, nitrogen, oxygen, argon, or methane
- **Operating pressure**: Variable for energy tuning (low for low-energy studies)
- **Magnetic fields**: 1000-2000 Gauss for momentum analysis

9.4.4 Particle Measurement Capabilities

Specific Ionization

- Alpha/protons: Dense, straight tracks
- Electrons/positrons: Thin, wispy trails
- Neutrons/gamma: Indirect detection via secondary particles

Momentum Analysis

$$p = 0.3BR$$

Where p = momentum (GeV/c), B = magnetic field (Tesla), R = track curvature (meters). Momentum change measured via lead plate insertion.

Mass Determination

Combines measurements of:

- Specific ionization density
- Particle range
- Magnetic curvature
- Momentum change rate

9.4.5 Nuclear Reaction Studies

- Conservation law verification (energy/momentum)
- Resonance level analysis of excited nuclei
- Alpha/beta/gamma spectra characterization
- Neutron energy measurement via proton recoils

Figure 9.4: Modular expansion chamber design with interchangeable components (Mound Lab, 1949)

9.4.6 Design Innovations

- **Variable expansion**: Adjustable rubber ring compression
- **Gas interchange system**: Multiple gas inlets for different stopping powers
- **Stereoscopic imaging**: Prism-mirror camera system for 3D track reconstruction
- **Electronic control**: Automated expansion, lighting, and camera sequencing

Chapter 10

Building your own Cloud Chamber

10.1 Materials Used

- Acrylic Sheets (12”x6”)
- Acrylic Sheets (12”x12”)
- Aluminium Tape
- Isopropyl Alcohol
- Heat Sink (150 x 60 mm)
- Heat Sink Gel
- Foam
- Glue
- Double Tape
- Camera

10.2 Basic Principles

The cloud chamber works by creating a supersaturated environment where isopropanol vapor is in a gaseous state at a temperature it normally cannot exist at. This supersaturation is achieved by evaporating isopropanol from a foam at the top of

the chamber and allowing it to sink towards a very cold heat sink at the bottom, which is cooled by the heat sink gel. When an electrically charged particle crosses this supersaturated vapor, it ionizes the gas molecules along its path by tearing away electrons, leaving these molecules positively charged. These charged molecules then act as condensation nuclei, causing small droplets of alcohol to form along the particle's path. The visible accumulation of these droplets forms the "tracks" that can be observed.

10.3 Design

The cloud chamber design involves a clear container made with acrylic sheets with foam attached to its bottom. This container is inverted and placed on a Heat sink. The Heat sink is filled with the heat sink gel which is cooled down. The foam inside the acrylic container is soaked with isopropanol. A light source illuminates the sensitive area just above the metal plate to make the tracks visible against the black background. The design is based on the "continuously sensitive diffusion cloud chamber" concept, utilizing heat sink to cool down the bottom of the chamber.

10.4 Working of our model

To operate the cloud chamber, first, prepare the heat sink;wrap it with aluminium tape ensure a high-contrast background and conductivity for viewing white particle tracks. Next, attach the foam to the bottom of the acrylic container using split pins. Apply heat sink gel to the heat sink and let it cool down for sometime. With plastic gloves and safety goggles on, soak the felt inside the acrylic container with pure isopropanol; tilt the

chamber to ensure the felt is fully saturated. Place the heat sink, ensuring the felt inside the acrylic container is already soaked. Finally, place the acrylic container upside down onto the cooled heat sink, fitting its walls into any grooves if present, which helps seal the box. After a few minutes for cooling and the formation of a stable sensitive area, a rain-like mist of alcohol will be visible. Turn off room lights and use torch lights to illuminate the alcohol mist directly above the metal plate. Within minutes, tracks of high-energy particles should become visible, appearing like thin spider's threads. Capture the images of the trails formed with the camera. Additional alcohol can be added through holes in the top of the box if needed.

10.5 Gallery

Figure 10.1: Making of the Cloud Chamber

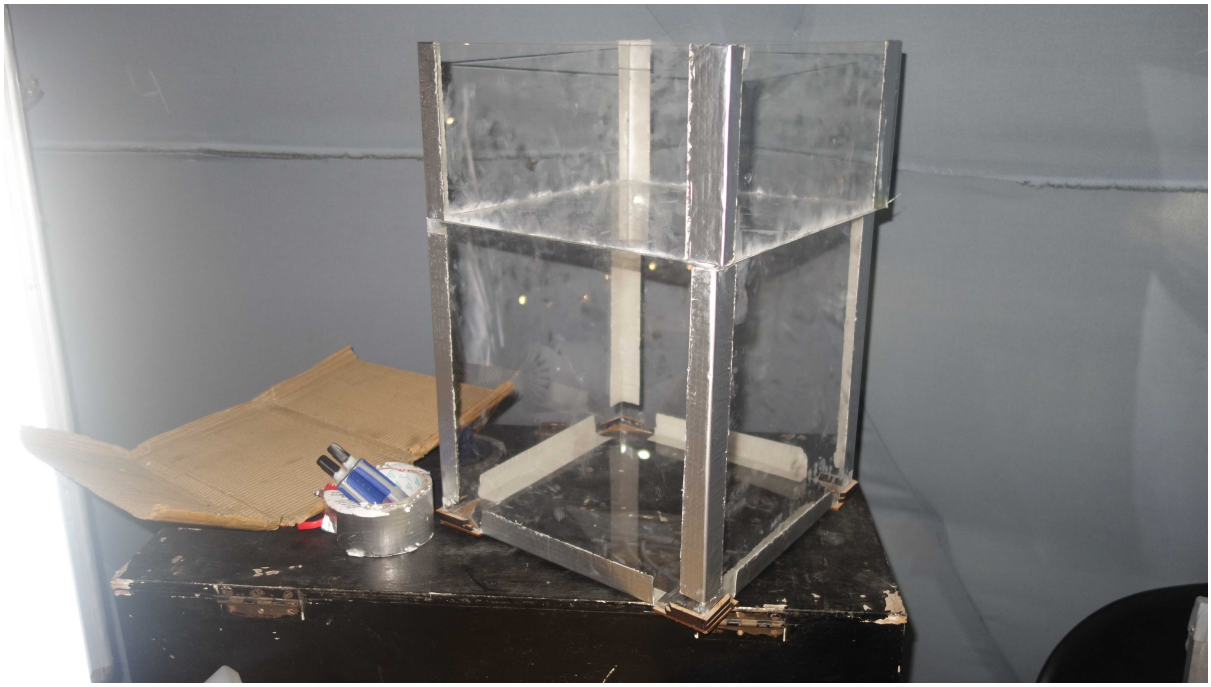

Figure 10.2: Finalised Acrylic structure